Hindawi
Advances in Materials Science and Engineering
Volume 2021, Article ID 5597415, 8 pages
https://doi.org/10.1155/2021/5597415

Research Article

Investigation of Structural, Electrical, and Vibrational Properties of $Bi_{1.98}A_{0.02}Fe_4O_9$ (A = Ba, Ce) Multiferroic Ceramics

Ashwini Kumar,[1] **Poorva Sharma**,[1] **Nikhil Bhardwaj**,[2] **Jingyou Tang**,[1] **and Guolong Tan**[1,3]

[1]*Key Laboratory of Multifunctional Materials, Department of Electronic Engineering, Luzhou Vocational and Technical College, Luzhou, Sichuan 646000, China*
[2]*School of Physics, Devi Ahilya University, Indore 452001, India*
[3]*Institute of New Materials, Wuhan University of Technology, Wuhan,430070, China*

Correspondence should be addressed to Ashwini Kumar; 101101216@seu.edu.cn and Poorva Sharma; poorva@nuaa.edu.cn

Received 31 January 2021; Revised 1 July 2021; Accepted 5 July 2021; Published 15 July 2021

Academic Editor: Francisco Javier Fernández Fernández

In this paper, we report the synthesis, phase formation, and basic characterization of polycrystalline $Bi_2Fe_4O_9$, $Bi_{1.98}Ba_{0.02}Fe_4O_9$, and $Bi_{1.98}Ce_{0.02}Fe_4O_9$ samples prepared by the sol-gel technique. The crystal structure of the prepared samples has been characterized by means of X-ray diffraction and Raman scattering spectroscopy. All the obtained XRD peaks can be indexed to the orthorhombic *Pbam* structure and reveal the formation of $Bi_2Fe_4O_9$. The Raman spectrum identifies A_g, B_{2g}, and B_{3g} active optical phonon modes. The crystallite size and morphology of the nanoparticles have been analyzed using scanning electron microscope (SEM). Dielectric constant (ε') decreases as the frequency increases, and it is constant at the higher frequency region which can be explained based on the ionic conduction phenomenon in the low frequency region. The ε' values of $Bi_2Fe_4O_9$(650–850), $Bi_2Fe_4O_9$(800–850), $Bi_{1.98}Ba_{0.02}Fe_4O_9$, and $Bi_{1.98}Ce_{0.02}Fe_4O_9$ samples at 10 Hz frequency are about 37, 75, 90, and 393, respectively. The observed properties signify that these materials are very useful in advanced technological and practical applications.

1. Introduction

In the past few years, there has been great attention in bismuth ferrite $Bi_2Fe_4O_9$ because of its potential applications in information and technology applications, digital memory, catalytic as well as in gas sensing [1, 2]. $Bi_2Fe_4O_9$ has an orthorhombic (space group *Pbam*) structure and belongs to family of mullite-type crystal structures [3, 4]. A unit cell of $Bi_2Fe_4O_9$ contains two formula units with evenly Fe ions distributed between octahedral (FeO_4) and tetrahedral (FeO_4) sites. In addition, Bi^{3+} ions are surrounded by eight oxygen ions. The perovskite $BiFeO_3$ (BFO), which is both FE ($T_{CE} = 1103$ K) and antiferromagnetic (AFM) ($T_N = 640$ K), is one of the well-known multiferroics [5]. However, it is difficult to obtain phase-pure BFO avoiding the formation of second phases during the conventional synthesis process. Various impurity phases have been reported to occur, such as $Bi_2Fe_4O_9$, $Bi_{46}Fe_2O_{72}$, and $Bi_{25}FeO_{40}$ [6, 7]. Among the impurity phases, $Bi_2Fe_4O_9$ is a well-known material, which has been extensively studied over the past several decades for various functional applications such as a semiconductor gas sensor and as a catalyst for ammonia oxidation [8, 9]. An unexpected multiferroic effect, which is observed as a coexistence of antiferromagnetism and ferroelectric polarization, was reported in $Bi_2Fe_4O_9$, attributed to the frustrated spin system coupled with phonons [10]. In the past, bulk $Bi_2Fe_4O_9$ were synthesized by solid-state reaction, and the multiferroic properties have been studied, displaying ferroelectric hysteresis loops at $T = 250$ K and antiferromagnetic (AFM) ordering $T_N = 260$ K [11]. It is also claimed that $Bi_2Fe_4O_9$ is one of the promising multiferroic materials. However, the evidence for ferroelectricity is not very strong. Few authors reported hysteresis data [5, 12, 13] in which the P-E field curves tend to give oval rather than ferroic-shaped hysteresis

loops. $Bi_2Fe_4O_9$ with a band gap of about 1.53 eV presents catalytic activity under visible light irradiation [14, 15].

Sol-gel processing, which gives a polycrystalline material, can control particle size of the crystallized phase and can eliminate any pores. We can also design the shape/form of precursor (bulk, thin-film, and so on) [16]. In addition, metastable phases, which are hardly synthesized via solid-state route, often crystallize in ceramics prepared by sol-gel route or hydrothermal method [17, 18]. Therefore, the processing has been studied intensively in order to produce the sophisticated functional materials. In recent times, Mohapatra et al. studied Ho^{3+} doped $Bi_2Fe_4O_9$samples and reported that Bi/Fe-site substitution in $Bi_2Fe_4O_9$ strongly affects its magnetic properties with the observation of an increase in the Neel temperature accompanied by the enhanced magnetodielectric coupling as compared with pure $Bi_2Fe_4O_9$ [19]. Verseils et al. investigated the magnetic and crystallographic transitions as well as spin-lattice coupling in the Cairo pentagonal magnet $Bi_2Fe_4O_9$ through infrared synchrotron-based spectroscopy as a function of temperature (20–300 K) and pressure (0–15.5 GPa) [20]. Liang et al. studied the structural, magnetic, and electrical properties of Ba-modified $Bi_2Fe_4O_9$ samples which were prepared by sol-gel method. They observed the significant enhancement in remnant magnetization, saturation magnetization, dielectric constant as well as conductivity due to substitution of Ba content in $Bi_2Fe_4O_9$ [21]. In an another recent work, $Bi_2Fe_4O_9$ and Gd-doped $Bi_2Fe_4O_9$ samples were synthesized by solid-state mechanochemical ball milling technique, and it revealed the remarkable changes in magnetic and dielectric properties for Gd-doped $Bi_2Fe_4O_9$ samples due to electron-hole hopping mechanism and spin-orbital coupling through D-M interaction. In addition, they also found that the Gd-doped $Bi_2Fe_4O_9$ samples had much higher photocatalytic degradation of MB dye than the undoped $Bi_2Fe_4O_9$ [22]. From the point of theory, Ameer et al. used the first-principle calculations to study the effect of 3*d* transition metal (TM) ions (Sc, Ti, V, Cr, Mn, Co, Ni, Cu, and Zn) on the structural, electronic, and magnetic properties of ferromagnetic $Bi_2Fe_4O_9$ and provided a comprehensive understanding of the possible effects of 3*d* TM dopants on $Bi_2Fe_4O_9$ [23].

Studies of electric and dielectric properties are important from both fundamental and application point of view. Dielectric and magnetic behavior of ferrites is greatly influenced by an order of magnitude of conductivity and is mostly dependent on the preparation method and sintering conditions [5, 24]. Sol-gel technique to prepare samples has been recognized as one of the most important synthetic methods, with the advantages of low cost, simple process, and controllable morphology. Therefore, the method of obtaining fine $Bi_2Fe_4O_9$ powder by the sol-gel method has become the goal of many researchers in this field. Therefore, in this paper, we have synthesized the pristine $Bi_2Fe_4O_9$ and $Ba^{2+}$and Ce^{3+} doped $Bi_2Fe_4O_9$by sol-gel technique to study their structural and physical properties. In order to obtain a suitable ceramic phase, we examined the phase formation and physical properties and the glassy precursor was subjected to different heat-treatments at different temperatures and for different durations. Despite the evident importance of $Bi_2Fe_4O_9$ as a functional material, very few reports have appeared. Here, we report the phase formation, physical properties, and vibrational properties of polycrystalline $Bi_2Fe_4O_9$ ceramic synthesized.

2. Experimental Details

2.1. Synthesis. $Bi_2Fe_4O_9$, $Bi_{1.98}Ba_{0.02}Fe_4O_9$, and $Bi_{1.98}Ce_{0.02}Fe_4O_9$ ceramics have been successfully synthesized by sol-gel route. All the chemicals are analytical grade and used without further purification. High purity nitrates such as $Bi(NO_3)_3.5H_2O$ and $Fe(NO_3)_3.9H_2O$ were carefully weighed and stoichiometrically mixed. It utilizes multifunctional organic acids capable of chelating metal ions into stable complexes. Suitable metal salts are introduced into the ethylene glycol, citric acid, which is added in large excess to form metal citrates.

$Bi_2Fe_4O_9$: The precursors of $Bi(NO_3)_3.5H_2O$ and $Fe(NO_3)_3.9H_2O$ are taken in a ratio (molar ratio) of 1:1. For 10 gm of sample, we weighed 12.3553 g $Bi(NO_3)_3.5H_2O$ and 20.5805 g $Fe(NO_3)_3.9H_2O$ precursors. Appropriate amount of deionized water is added to dissolve, and then the solution is stirred on a magnetic stirrer. While stirring, citric acids ($C_6H_8O_7$) are introduced in 1.5 : 1 M ratio with respect to the metal nitrates as a complexing agent and maintained the pH value (6-7) of mixed solution by adding ammonia [11]. Temperature was supplied to allow the gel to form up to a temperature of 100°C, and the xero-gel was completely burned into ash. It was then calcined at 650°C for 2 hours. For the same powder, we carried out the second calcination at 850°C for 2 hours and observed its changes. In another heating treatment, the calcination was done at 800°C and then calcined at 850°C again after grinding. The powder obtained was then ground in agate mortar and pestle. Finally, powder products were reground and pressed into the pellets and then sintered in a muffle furnace at temperature 850°C for 8 hours.

Ba and Ce-doped $Bi_2Fe_4O_9$: Nitrate precursors of Bi, Fe, Ba, and Ce (i.e., $Bi(NO_3)_3.5H_2O$ and $Fe(NO_3)_3.9H_2O$, $Ba(NO_3)_2$, and $Ce(NO_3)_3.6H_2O$) are taken in 1 : 1 molar ratio. Appropriate deionized water was added to dissolve, and solution was then stirred on magnetic stirrer. During stirring, we have added the citric acid ($C_6H_8O_7$) in 1.5 : 1 M ratio with respect to the metal nitrates as complexant, and the solution was adjusted to a pH value ~6-7 by addition of ammonia. Temperature was supplied to form gel up to 100°C and after that xero-gel was completely burned to form ash. First calcination was done at 650°C, and second calcination was done at 850°C with intermediate grinding. Finally, the pellets were sintered in a muffle furnace at the temperature of 850°C for 8 hours.

2.2. Experimental Techniques. In order to study the crystal structure and phase formation, we obtained the X-ray diffraction (XRD) pattern for the powder samples using a Bruker D8 Advance X-ray diffractometer with a step size of 0.02° and CuKα (1.5406 Å) radiation. The surface morphology of the prepared samples (pellet form) was investigated using a JEOL, JSM-5600 scanning electron microscope. Further, the particle sizes were estimated from SEM micrographs using ImageJ software. Raman measurements on as synthesized sample were carried out on Jobin-Yovn Horiba LABRAM (System HR800) spectrometer with a 632.8 nm excitation source equipped with a Peltier cooled CCD detector. Dielectric measurements were made as a function of frequency in the range of 1 Hz–10 MHz on the Novocontrol alpha-ANB impedance analyzer at room temperature. The dielectric measurements were performed on the circular pellet (10 mm diameter and 1 mm thickness) samples with silver paint coated on two sides as the electrodes. The real (ε') and imaginary (ε'') parts of the complex dielectric constant were calculated from raw data and the pertinent sample dimensions as follows:

$$c_0 = \varepsilon_0 \frac{A}{d},$$
$$\varepsilon' = \frac{C\,d}{\varepsilon_0 A}, \quad (1)$$
$$\varepsilon'' = \varepsilon \tan{}' \delta,$$

where C is the capacitance, d is the thickness of the pellet, A is the area of sintered pellet, and ε_0 is the permittivity of vacuum.

3. Results and Discussion

3.1. Crystal Structure Analysis. Figure 1 shows the X-ray powder diffraction (XRD) pattern of pristine $Bi_2Fe_4O_9$, Ba, and Ce-doped $Bi_2Fe_4O_9$ samples carried out at room temperature. As we mentioned before, the $Bi_2Fe_4O_9$ samples were calcined at different temperatures and are further designated as $Bi_2Fe_4O_9$(650–850) for $Bi_2Fe_4O_9$ calined at 650°C and 850°C and $Bi_2Fe_4O_9$(800–850) for $Bi_2Fe_4O_9$ sample calcined at 800°C and 850°C. Finally, these both samples have been sintered at 850°C for 8 hours. For the samples $Bi_2Fe_4O_9$(650–850) and $Bi_2Fe_4O_9$(800–850), the diffraction peaks are well indexed with the orthorhombic structure of $Bi_2Fe_4O_9$ (space group: *Pbam*) and match well with JCPDS card No. 74–1098 [25]. These results confirm that phase-pure $Bi_2Fe_4O_9$ can be synthesized by sol-gel route. The XRD peak close to 11° is of bismuth due to the presence of $Bi(NO_3)_3.5H_2O$ [26]. From (a) and (b) in Figure 1, we can observe the broading of the peaks in $Bi_2Fe_4O_9$(650–850) sample due to low calcination temperature, whereas due to high calcination temperature, proper crystalline phase has been observed in $Bi_2Fe_4O_9$(800–850) sample. Due to calcination temperature variation, double peaks transform into a single peak from sample $Bi_2Fe_4O_9$(650–850) to $Bi_2Fe_4O_9$(800–850). Furthermore, the refined lattice parameters of sample $Bi_2Fe_4O_9$(650–850) are $a = 7.94$ Å, $b = 8.40$ Å, and $c = 5.92$ Å and $a = 7.95$ Å, $b = 8.45$ Å, and $c = 5.94$ Å for $Bi_2Fe_4O_9$(800–850), revealing the slight expansion in both the *ab* plane and the *c* axis with doping contents increasing. In addition, with the increase in calcination temperature, there is a limited intensity increasing and narrowing of the diffraction peaks, indicative of better crystallization and the increase in crystalline sizes. Using the Debye Scherrer formula, the average crystalline size can be estimated to be about 52 nm, 80 nm for $Bi_2Fe_4O_9$(650–850) and $Bi_2Fe_4O_9$(800–850).

XRD for alkaline earth metal Ba^{+2} ion and rare earth Ce^{+3} ion-doped $Bi_2Fe_4O_9$ ceramics are shown in (c) and (d) of Figure 1. For the doped samples, the diffraction peaks are well indexed with the orthorhombic structure of $Bi_2Fe_4O_9$ (space group: *Pbam*) and matche well with (JCPDS: 25–0090). As witnessed from (c) and (d) in Figure 1 in the doped $Bi_2Fe_4O_9$samples, there is a shift in lower theta value due to ionic radius mismatch of dopent (ionic radius of Ba = 1.35 and Ce = 1.01) with Bi^{+3} (0.96) ion. The ionic radius of Ba and Ce ions is greater than that of Bi ion; that is why we are getting a shifting at lower theta value as compared with parent $Bi_2Fe_4O_9$ ceramic. The lattice parameters were obtained using indexing such as $a = 7.101$ Å, $b = 8.50$ Å, and $c = 5.94$ Å for $Bi_{1.98}Ba_{0.02}Fe_4O_9$ and $a = 7.99$ Å, $b = 8.48$ Å, and $c = 5.93$ Å for $Bi_{1.98}Ce_{0.02}Fe_4O_9$ sample. The crystalline size for Ce^{+3} and Ba^{+2} ions-doped ceramics is found to be 62 and 65 nm, respectively.

3.2. Microstructure Analysis. As the dielectric, optical, and magnetic properties are highly dependent on composition and microstructure acquired by the samples, we used the scanning electron microscope (SEM) to study the surface morphological and microstructural characteristics of pristine and doped $Bi_2Fe_4O_9$ compounds. Figures 2–2 show typical SEM images of $Bi_2Fe_4O_9$(650–850), $Bi_2Fe_4O_9$(800–850), $Bi_{1.98}Ba_{0.02}Fe_4O_9$, and $Bi_{1.98}Ce_{0.02}Fe_4O_9$ samples, respectively. Compared with the pristine $Bi_2Fe_4O_9$ sample, the grains of the doped $Bi_2Fe_4O_9$ sample are randomly oriented and have the smaller grain size. We determined average grain size using ImageJ Software and found to be nearly 0.8–1.2 micrometer. As we can see in the SEM images, the micrograph revealed that $Bi_2Fe_4O_9$ materials mostly consist of nonuniform grains and each grain is interconnected edge by edge. Distribution of grains is homogeneous and agglomerations of the particles. Samples seem to be porous in nature, which is expected to highly influence the dielectric properties. Therefore, we can say that the particle size increases with increase in the calcination temperature as we can see in SEM image of $Bi_2Fe_4O_9$(800–850) sample. The typical SEM images reveal that microstructures comprise of nonuniform grains with varying particles size indicating polycrystalline nature of as-prepared samples [27].

3.3. Raman Scattring Analysis. The Raman spectrum of $Bi_2Fe_4O_9$ at room temperature is depicted in Figure 3. The Raman active modes of the structure can be summarized using the irreducible representation $12Ag + 12B1gv9B2g + 9\ B3g$, which is employed to describe Raman modes of orthorhombic

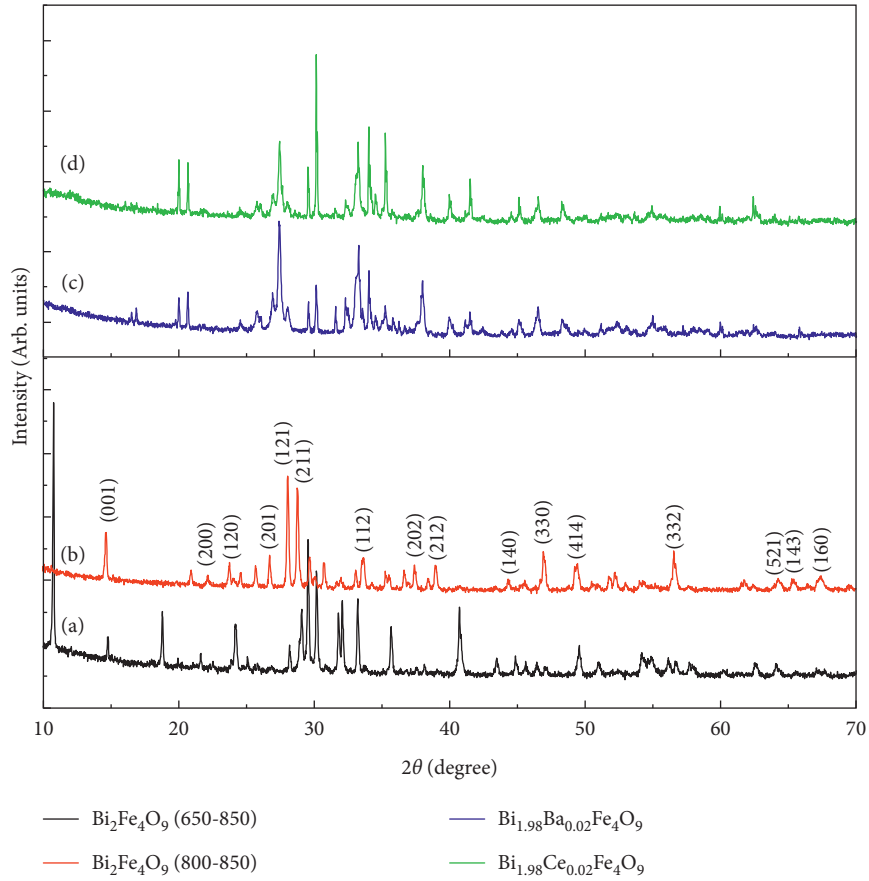

FIGURE 1: Room temperature XRD pattern for (a) $Bi_2Fe_4O_9$(650–850), (b) $Bi_2Fe_4O_9$(800–850), (c) $Bi_{1.98}Ba_{0.02}Fe_4O_9$, and (d) $Bi_{1.98}Ce_{0.02}Fe_4O_9$ samples.

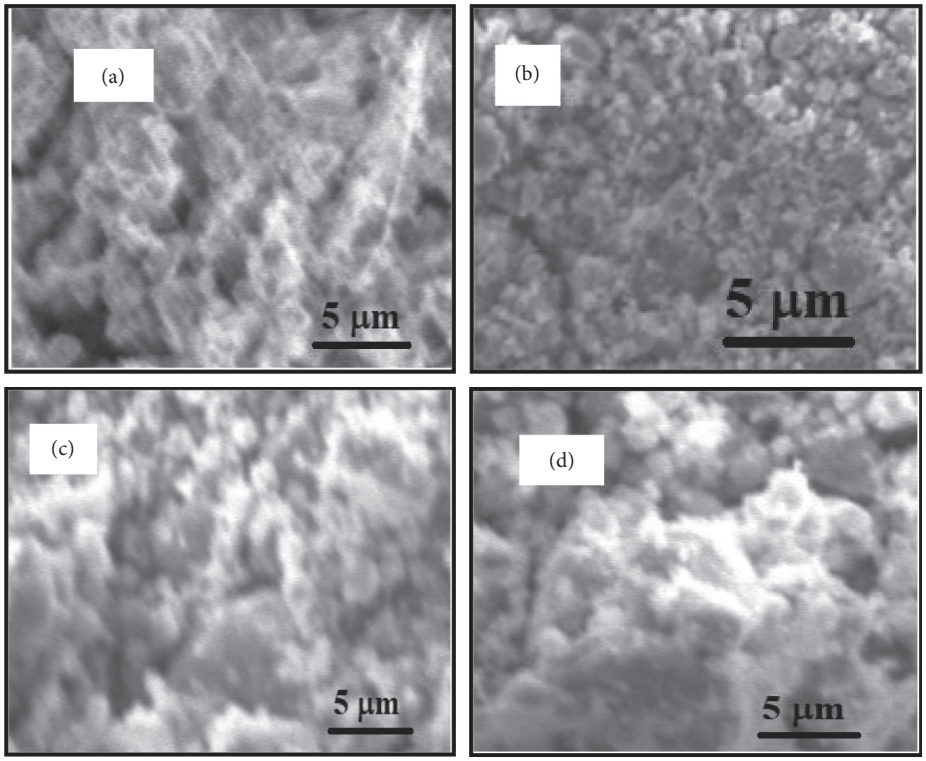

FIGURE 2: Scanning electron microscope (SEM) images of the as-prepared $Bi_2Fe_4O_9$-based samples: (a) $Bi_2Fe_4O_9$(650–850), (b) $Bi_2Fe_4O_9$(800–850), (c) $Bi_{1.98}Ba_{0.02}Fe_4O_9$, and (d) $Bi_{1.98}Ce_{0.02}Fe_4O_9$ samples.

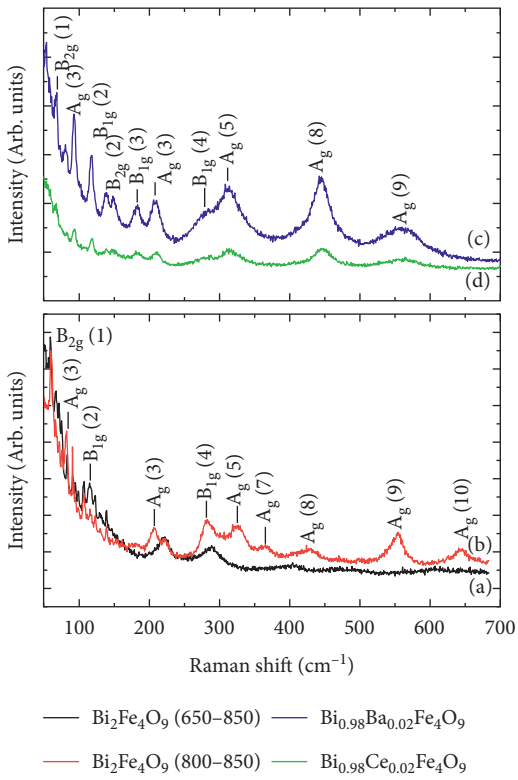

FIGURE 3: Raman spectra for (a) $Bi_2Fe_4O_9$(650–850), (b) $Bi_2Fe_4O_9$(800–850), (c) $Bi_{1.98}Ba_{0.02}Fe_4O_9$, and (d) $Bi_{1.98}Ce_{0.02}Fe_4O_9$ samples.

(*Pbam* space group) [25]. In the measured Raman spectra of $Bi_2Fe_4O_9$(650–850), the A_g modes existed at 83, 95, 115, 122, 139, 222, 289, and 607 cm^{-1}. The agreement between experimental and predicted values is relatively good for the all frequency modes, dominated by Bi vibrations. The Raman peak centered at 472 cm^{-1} might be attributed to magnetic ordering effect on phonon line width consistent with earlier observation of bands at ~260 and 472 cm^{-1} due to magnon scattering. Similarly, for $Bi_2Fe_4O_9$(800–850), the obtained Raman A_g modes are at 91, 206, 282, 326, 365, 430, 554, and 640 cm^{-1}. We can analyze that there are number of modes decreasing due to increase in calcination temperature. The A_g modes for $Bi_{1.98}Ba_{0.02}Fe_4O_9$ are as follows (53, 93, 119, 183, 209, 313, 446, and 558 cm^{-1}). Similarly, for $Bi_{1.98}Ce_{0.02}Fe_4O_9$, the A_g modes are at 53, 68, 118, 183, 206, 308, 442, and 560 cm^{-1}. It would be more practical to study the magnetic excitations in $Bi_2Fe_4O_9$ under the assumption that they involve two-magnon processes, like in the well-known cases of ferrites [28] or cuprates [11, 29]. At higher frequency (>250 cm^{-1}), it is unlikely that the magnetic-order-induced bands correspond to one-magnon excitations but rare-earth orthoferrites ($RFeO_3$; R = Dy, Ho, Er, Sm, and so on) have frequencies below 25 cm^{-1} for comparison of the zone-center magnons [30].

3.4. Dielectric Response. Figure 4 illustrates the frequency dependence of dielectric constant (ε') for $Bi_2Fe_4O_9$ ceramics in the frequency range of 1 Hz to 10 MHz with room temperature. As observed from Figure 4, the dielectric constant (ε') decreases with increase in frequency and almost constant at high frequency due to dielectric relaxations in all prepared samples. The observed high value of dielectric constant and dielectric loss at low frequencies indicates the presence of significant *dc* conductivity, which may be due to space charge polarization that originated from oxygen vacancies, bismuth vacancies, and so on [31]. In general, the dipolar, electronic, ionic, and interfacial polarizations have effect on the dielectric constant of any material. At low frequencies, dipolar polarization and interfacial polarization are effective for the dielectric constant. However, at higher frequencies, the electronic polarization is effective and the dipolar contribution becomes insignificant. The decrease in dielectric constant with increased frequency could be explained based on the phenomenon of dipole relaxation. When the sample is placed under the field, charge carriers move freely within the crystal grains but contain at the boundary and temporarily stop until they pass the boundary. This will result in the formation of potential barrier across the sample and gets polarized. Therefore, it was found that the dielectric constant decreases with increasing frequency [32]. At higher frequencies, the decrease in the dielectric constant is obvious due to lagging behind of applied field. Beyond the certain frequencies, dipoles do not respond to the applied field and thus remain nearly constant.

The value of dielectric constant (ε') for all $Bi_2Fe_4O_9$-based sintered samples at frequency of 10 Hz has been found to be 37, 75, 90, and 393 for $Bi_2Fe_4O_9$(650–850), $Bi_2Fe_4O_9$(800–850), $Bi_{1.98}Ba_{0.02}Fe_4O_9$, and $Bi_{1.98}Ce_{0.02}Fe_4O_9$, respectively, whereas the value of dielectric constant (ε') at higher frequency of 1 MHz has been found to be 11.68, 12.90, 5.06, and 5.36 for $Bi_2Fe_4O_9$(650–850), $Bi_2Fe_4O_9$(800–850), $Bi_{1.98}Ba_{0.02}Fe_4O_9$, and $Bi_{1.98}Ce_{0.02}Fe_4O_9$ samples, respectively. As shown in Figure 4, dielectric constant ε' relatively increases with increasing sintering temperature confirming that it exhibits space charge polarization, and it can be explained with the help of the Maxwell–Wagner effect. These results appear to be consistent with previous empirical analysis using the Maxwell–Wagner model with thermal activation across multiple band gaps in isolated impurities [33, 34]. Apart from this, it is observed that the dielectric constant shows enhancement after Ba and Ce substitution in $Bi_2Fe_4O_9$ at lower frequencies as compared with pristine $Bi_2Fe_4O_9$. This increase may be ascribed to large number of defects due to Ba and Ce doping in $Bi_2Fe_4O_9$ lattice. However, at higher frequencies, the dielectric constant shows reduction in the value and is obvious due to lagging behind the applied field. It can be noticed that Ba and Ce additions to $Bi_2Fe_4O_9$ lattice help to improve the dielectric constant. Figure 5 represents the dielectric loss (tanδ) as a function of frequency of $Bi_2Fe_4O_9$-based ceramics at room temperature. Furthermore, Ba and Ce-doped $Bi_2Fe_4O_9$ exhibited higher value of dielectric constant and dielectric loss as compared with pristine $Bi_2Fe_4O_9$ due to large off-center displacement of Fe^{3+} ions in octahedral and reduced particle size [35]. As the hopping process of conducting electrons and holes increases, the band gap decreases and the conductivity increases [36]. We have observed that the value of dielectric loss is low for $Bi_2Fe_4O_9$(650–850) among the entire prepared sample, and dielectric relaxation is possible in all prepared samples.

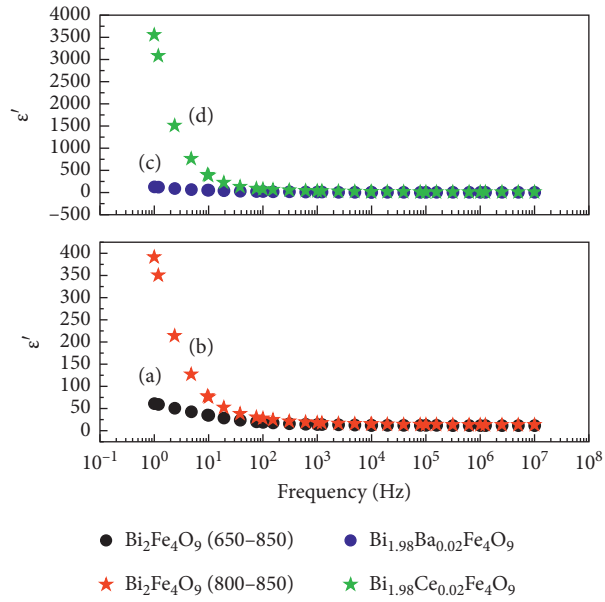

Figure 4: Dielectric constant behavior for $Bi_2Fe_4O_9$(650–850), $Bi_2Fe_4O_9$(800–850), $Bi_{1.98}Ba_{0.02}Fe_4O_9$, and $Bi_{1.98}Ce_{0.02}Fe_4O_9$ samples.

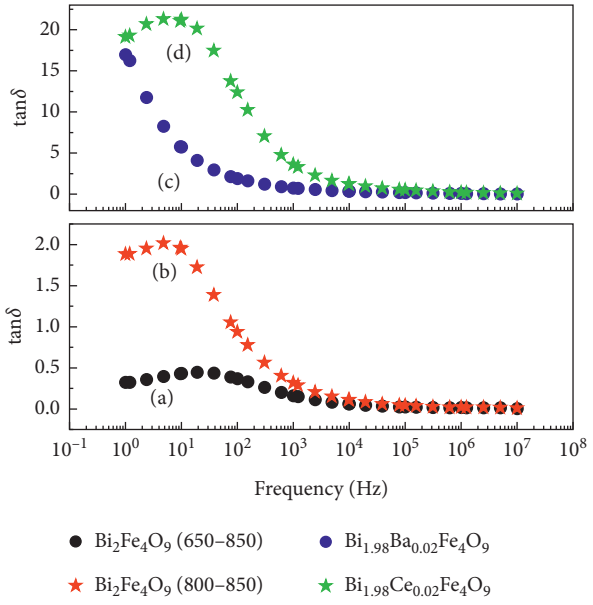

Figure 5: Dielectric loss behavior for $Bi_2Fe_4O_9$(650–850), $Bi_2Fe_4O_9$(800–850), $Bi_{1.98}Ba_{0.02}Fe_4O_9$, and $Bi_{1.98}Ce_{0.02}Fe_4O_9$ samples.

4. Conclusions

In conclusion, the polycrystalline samples of $Bi_2Fe_4O_9$(650–850), $Bi_2Fe_4O_9$(800–850), $Bi_{1.98}Ba_{0.02}Fe_4O_9$, and $Bi_{1.98}Ce_{0.02}Fe_4O_9$ samples were successfully prepared by sol-gel route. By the indexing of X-ray diffraction data, the formation of $Bi_2Fe_4O_9$ phase having orthorhombic structure with *Pbam* space group is confirmed. There is no evidence for structural change in the prepared samples. Raman spectra reveal that the presence of magnon peak is only in $Bi_2Fe_4O_9$(650–850) sample. The value of ε' for all $Bi_2Fe_4O_9$-based $Bi_2Fe_4O_9$(650–850), $Bi_2Fe_4O_9$(800–850), $Bi_{1.98}Ba_{0.02}Fe_4O_9$, and $Bi_{1.98}Ce_{0.02}Fe_4O_9$ samples is about 37, 75, 90, and 393, respectively, at frequency of 10 Hz. At higher frequency of 1 MHz, the values of ε' are 11.68, 12.90, 5.06, and 5.36 for $Bi_2Fe_4O_9$(650–850), $Bi_2Fe_4O_9$(800–850), $Bi_{1.98}Ba_{0.02}Fe_4O_9$, and $Bi_{1.98}Ce_{0.02}Fe_4O_9$ samples, respectively. Dielectric constant (ε') decreases with increasing frequency and becomes almost constant at high frequency region. The value of dielectric loss is low for $Bi_2Fe_4O_9$(650–850) among the entire prepared sample, and dielectric relaxation is possible in all as-prepared samples. The decrease in dielectric constant with increased frequency could be explained on the basis of the ionic conduction phenomenon in the low frequency region. These properties make this material very useful in technological and practical applications.

Data Availability

The data used to support the findings of this study are available from the corresponding author upon request.

Conflicts of Interest

The authors declare that they have no conflicts of interest regarding the publication of this study.

Acknowledgments

The authors acknowledge the financial support from National Natural Science Foundation of China under grant no. 11774276. Kumar and Sharma acknowledge the Luzhou Vocational and Technical College for providing them start-up research grants and support and also acknowledge the Luzhou Talent Work Leading Group Office for job-incentive and resettlement subsidies for high-level talents. The authors are grateful to Dr. S. Satapathy for their long-term collaboration and numerous fruitful discussions.

References

[1] G. Wang, S. Yan, J. Sun, S. Wang, and Q. Deng, "Visible light photocatalytic and magnetic properties of Nd doped $Bi_2Fe_4O_9$ powders," *Journal of Materials Science: Materials in Electronics*, vol. 28, no. 5, pp. 4371–4377, 2016.

[2] N. I. Zakharchenko, "Catalytic properties of the Fe_2O_3–Bi_2O_3 system in ammonia oxidation to nitrogen oxides," *Kinetics and Catalysis*, vol. 43, no. 1, pp. 95–98, 2002.

[3] Y. Xiong, M. Wu, Z. Peng, N. Jiang, and Q. Chen, "Hydrothermal synthesis and characterization of $Bi_2Fe_4O_9$ nanoparticles," *Chemistry Letters*, vol. 33, no. 5, pp. 502-503, 2004.

[4] Y. Takahashi, K. Nakamura, M. Osada, and T. Fujiwara, "Structural relaxation and quasi-elastic light scattering in glass: A," *Scientific Reports*, vol. 2, no. 1, p. 714, 2012.

[5] A. K. Singh, S. D. Kaushik, B. Kumar et al., "Substantial magnetoelectric coupling near room temperature in $Bi_2Fe_4O_9$," *Applied Physics Letters*, vol. 92, no. 13, Article ID 132910, 2008.

[6] M. M. Kumar, A. Srinivas, and S. V. Suryanarayana, "Structure property relations in $BiFeO_3$/$BaTiO_3$ solid solutions," *Journal of Applied Physics*, vol. 87, no. 2, pp. 855–862, 2000.

[7] S. M. Selbach, M.-A. Einarsrud, and T. Grande, "On the TS," *Chemistry of Materials*, vol. 21, no. 1, pp. 169–173, 2009.

[8] H. Koizumi, N. Niizeki, and T. Ikeda, N. I. Zakharchenko, "Russian journal of applied chemistry," *Jappense journal Applied Physics*, vol. 3, p. 495, 1964.

[9] A. S. Poghossian, H. V. Abovian, P. B. Avakian, S. H. Mkrtchian, and V. M. Haroutunian, "Bismuth ferrites: n," *Sensors and Actuators B: Chemical*, vol. 4, no. 3-4, pp. 545–549, 1991.

[10] T. Honma, N. Ito, T. Togashi, A. Sato, and T. Komatsu, "Triclinic Na2−xFe1+x/2P2O7/C glass-ceramics with high current density performance for sodium ion battery," *Journal of Power Sources*, vol. 227, pp. 31–34, 2013.

[11] A. P. Litvinchuk, L. BO, C. Thomsen, and C. W. Chu, "Magnetic excitations in $PrBa_2Cu_4O_8$ explored by Raman scattering," *Physica Status Solidi (B)*, vol. 215, no. 1, pp. 507–512, 1999.

[12] Z. M. Tian, S. L. Yuan, X. L. Wang et al., "Size effect on magnetic and ferroelectric properties in $Bi_2Fe_4O_9$ multiferroic ceramics," *Journal of Applied Physics*, vol. 106, no. 10, Article ID 103912, 2009.

[13] K. J. D. MacKenzie, T. Dougherty, and J. Barrel, "The electronic properties of complex oxides of bismuth with the mullite structure," *Journal of the European Ceramic Society*, vol. 28, no. 2, pp. 499–504, 2008.

[14] S. R. Mohapatra, B. Sahu, T. Badapanda, M. S. Pattanaik, S. D. Kaushik, and A. K. Singh, "Optical, dielectric relaxation and conduction study of $Bi_2Fe_4O_9$ ceramic," *Journal of Materials Science: Materials in Electronics*, vol. 27, no. 4, pp. 3645–3652, 2016.

[15] Q. Zhang, W. Gong, J. Wang et al., "Size-dependent magnetic, photoabsorbing, and photocatalytic properties of single-crystalline $Bi_2Fe_4O_9$ semiconductor nanocrystals," *Journal of Physical Chemistry C*, vol. 115, no. 51, pp. 25241–25246, 2011.

[16] A. Sakamoto and S. Yamamoto, "Glass-ceramics: engineering principles and applications," *International Journal of Applied Glass Science*, vol. 1, no. 3, pp. 237–247, 2010.

[17] T. Furukawa and W. B. White, "Raman spectroscopic investigation of the structure and crystallization of binary alkali germanate glasses," *Journal of Materials Science*, vol. 15, no. 7, pp. 1648–1662, 1980.

[18] K. Shioya, T. Komatsu, H. G. Kim, R. Sato, and K. Matusita, Y. Wang, G. Xu, L. Yang, Z. Ren, X. Wei, W. Weng et al., "Optical properties of transparent glass-ceramics in K_2O-Nb_2O_5-TeO_2 glasses," *Journal of Non-crystalline Solids*, vol. 189, no. 1-2, pp. 16–24, 1995.

[19] S. R. Mohapatra, P. N. Vishwakarma, S. D. Kaushik, and A. K. Singh, "Effect of Holmium substitution on the magnetic and magnetodielectric properties of multiferroic $Bi_2Fe_4O_9$," *Journal of Applied Physics*, vol. 122, no. 13, Article ID 134103, 2017.

[20] M. Verseils, A. P. Litvinchuk, J.-B. Brubach et al., "Infrared phonon spectroscopy on the Cairo pentagonal antiferromagnet $Bi_2Fe_4O_9$: a study through the pressure-induced structural transition," *Physical Review B*, vol. 103, no. 17, Article ID 174403, 2021.

[21] Y. Y. Liang, J. X. Lei, X. X. Wang, L. G. Wang, and C. M. Zhu, "Structure, magnetic and electrical properties of Ba-modified $Bi_2Fe_4O_9$," *Journal of Materials Science: Materials in Electronics*, vol. 30, no. 2, pp. 1691–1698, 2019.

[22] K. Subha Rao, S. Manjunath Kamath, R. Rajesh Kumar et al., "Delineating the photocatalytic properties of doped mullite $Bi_2Fe_4O_9$ by virtue of Gd^{3+} ions," *Materials Letters*, vol. 297, Article ID 129960, 2021.

[23] S. Ameer, K. Jindal, M. Tomar, P. K. Jha, and V. Gupta, "Tunable electronic and magnetic properties of 3d transition metal doped $Bi_2Fe_4O_9$," *Journal of Magnetism and Magnetic Materials*, vol. 509, Article ID 166893, 2020.

[24] M. Pooladi, I. Sharifi, and M. Behzadipour, "A review of the structure, magnetic and electrical properties of bismuth ferrite ($Bi_2Fe_4O_9$)," *Ceramics International*, vol. 46, no. 11, pp. 18453–18463, 2020.

[25] Y. A. Park, K. M. Song, and N. Hur, "Frequency-dependent dielectric anomalies in magnetic oxides," *Journal of the Korean Physical Society*, vol. 53, no. 6, pp. 3356–3360, 2008.

[26] L. Tröbs, M. Wilke, W. Szczerba, U. Reinholz, and F. Emmerling, "Mechanochemical synthesis and characterisation of two new bismuth metal organic frameworks," *CrystEngComm*, vol. 16, p. 5560, 2014.

[27] N. Bajpai, M. Saleem, and A. Mishra, "Effect of bismuth (Bi^{3+}) substitution on structural, optical, dielectric and magnetic nature of La_2CoMnO_6 double perovskite," *Journal of Materials Science: Materials in Electronics*, vol. 32, no. 10, pp. 12890–12902, 2021.

[28] M. J. Massey, U. Baier, R. Merlin, and W. H. Weber, "Effects of pressure and isotopic substitution on the Raman spectrum of α-Fe_2O_3: i," *Physical Review B*, vol. 41, no. 11, pp. 7822–7827, 1990.

[29] J. Holmlund, C. S. Knee, J. Andreasson, M. Granath, A. P. Litvinchuk, and L. Börjesson, "Two-magnon Raman scattering from the Cu_3O_4 layers in $(Sr_2,Ba_2)Cu_3O_4Cl_2$," *Physical Review B: Condensed Matter*, vol. 79, Article ID 085109, 2009.

[30] R. M. White, R. J. Nemanich, and C. Herring, "Light scattering from magnetic excitations in orthoferrites," *Physical Review B*, vol. 25, no. 3, pp. 1822–1836, 1982.

[31] M. R. Islam, M. S. Islam, M. A. Zubair, H. M. Usama, M. S. Azam, and A. Sharif, "Evidence of superparamagnetism and improved electrical properties in Ba and Ta co-doped $BiFeO_3$ ceramics," *Journal of Alloys and Compounds*, vol. 735, pp. 2584–2596, 2018.

[32] M. Soosen Samuel, J. Koshy, A. Chandran, and K. C. George, R. Kant, R. Singh, A. Bansal, and A. Kumar, "Dielectric behavior and transport properties of ZnO nanorods," *Physica B:*

Condensed Matter, vol. 406, no. 15-16, pp. 3023–3029, Article ID 114726, 2011.

[33] A. Shukla and R. N. P. Choudhary, "Study of electrical properties of La^{3+}/Mn^{4+}-modified $PbTiO_3$ nanoceramics," *Journal of Materials Science*, vol. 47, no. 13, pp. 5074–5085, 2012.

[34] R. R. Awasthi and B. Das, "Effect of temperature on physical properties of $Bi_2Fe_4O_9$ polycrystalline materials," *Journal of the Australian Ceramic Society*, vol. 56, no. 1, pp. 243–250, 2020.

[35] B. K. Vashisth, J. S. Bangruwa, S. P. Gairola, and V. Verma, "Structural, dielectric, ferroelectric and magnetic properties of Gd doped $BiFeO_3$," *Integrated Ferroelectrics*, vol. 194, no. 1, pp. 21–27, 2018.

[36] M. Umar, N. Mahmood, S. U. Awan, and S. Fatima, "Rationally designed La and Se co-doped bismuth ferrites with controlled bandgap for visible light photocatalysis," *RSC Advances*, vol. 9, pp. 17148–21715, 2019.